Theory of thermoelastic damping in electrostatically actuated microstructures

Sudipto K. De and N. R. Aluru
Department of Mechanical Science and Engineering, Beckman Institute for Advanced Science and Technology, University of Illinois at Urbana-Champaign, 405 N. Mathews Avenue, Urbana, Illinois 61801, USA
(Received 6 July 2006; published 17 October 2006)

Thermoelastic damping (TED) is an inherent energy dissipation mechanism in micromechanical resonators which imposes an upper limit on the quality factor. Micromechanical resonators with very high quality factors are essential for many applications. Electrostatic actuation is a very common mode of actuation for microresonators and microstructures (referred to as electrostatic microelectromechanical systems). The nonlinear electrostatic actuation force can significantly alter the nature of thermoelastic damping, and hence the quality factor Q_{TED} of the microstructures, from that predicted by the classical theory of thermoelastic damping developed by Zener [Phys. Rev. **52**, 230 (1937); **53**, 90 (1938)] and later improved by Lifshitz and Roukes [Phys. Rev. B **61**, 5600 (2000)]. In this paper, the classical theory of thermoelastic damping is modified for application to microstructures under arbitrary electrostatic actuation. The higher-order harmonics of the excitation frequency, which can be present in the oscillations due to the nonlinear nature of the electrostatic force, are taken into account in the modified theory. A physical level simulation tool is also developed in this paper based on coupled electrostatic, fluidic, and large-deformation thermoelastic analysis and validated by comparing with experimental data. The simulation results from the physical level analysis are compared with the predictions of the classical theory and the modified theory under electrostatic actuation. While significant differences (both quantitative and qualitative) are observed in the thermoelastic quality factor Q_{TED} obtained from the physical level simulations and the classical theory, the modified theory is in close agreement with the physical level analysis for the entire range of excitation frequencies considered.

DOI: 10.1103/PhysRevB.74.144305 PACS number(s): 85.85.+j, 05.45.−a, 65.40.De

I. INTRODUCTION

Electrostatically actuated microstructures [popularly known as electrostatic microelectromechanical systems (MEMS)] find widespread applications as ultrafast and high-precision actuators and sensors. Some examples of MEMS are accelerometers,[4] inertial sensors,[5] chemical sensors,[6] and rf filters and oscillators.[7] The quality factor, which is a measure of the amount of energy stored in the system compared to the energy dissipated by the system,[1] is an important design parameter for many MEMS applications. A high quality factor results in reduced readout errors, lower power requirements, improved stability, and increased sensitivity[8] for the system. As a result, it is very important to understand the dominant energy dissipation mechanisms in microresonators and to identify those that are fundamental as they can impose an upper limit on the quality factor. Thermoelastic damping (TED) is one such fundamental dissipation mechanism that is inherent to the system and cannot be completely eliminated by improved design or fabrication.[3] Thermoelastic damping in single-crystal silicon[9] and silicon nitride[10] microbeams at room temperature has been studied. The effect of the microbeam material properties on thermoelastic damping in fine-grained polysilicon flexural beams[11] and in trench-refilled polysilicon beams[12] has also been studied both theoretically and experimentally. The studies performed in Refs. 9, 10, and 12 were all based on the classical theory of thermoelastic damping developed by Zener[1,2] which is applicable for beams undergoing simple harmonic motion in the flexural mode. Finite-element-based physical level models have been developed for evaluating the thermoelastic damping and quality factor of MEMS devices with complex geometries like gyroscopes[8,13] where Zener's theory (applicable for beams) is not accurate. These physical level models[8,13] perform a thermo-mechanical analysis in the absence of any electrostatic forces. In this paper, thermoelastic damping in microstructures under electrostatic actuation (the most commonly used mode of actuation in MEMS) is studied. The nonlinear electrostatic force can give rise to complex (non-simple-harmonic) oscillations under extreme[14] or even under normal operating conditions[15] and for these cases the thermoelastic damping cannot be predicted accurately by the classical theory (neither the original Zener theory nor the improved Lifshitz and Roukes theory[3]). The classical theory of thermoelastic damping is modified in this paper to predict TED in MEMS under electrostatic actuation. The effect of the complex oscillations on the quality factor due to thermoelastic damping in MEMS is also studied here through an accurate and validated full-scale numerical simulation tool based on coupled electrostatic, fluidic, and large-deformation thermoelastic analysis.

The rest of the paper is outlined as follows. Section II presents the classical theory of thermoelastic damping that has been used extensively for computing the quality factor due to TED in MEMS, and Sec. III presents the modified theory and the physical models for thermoelastic damping in MEMS under electrostatic actuation. Comparisons between the classical theory, the modified theory, and numerical simulation results (using the physical models) on TED in MEMS under electrostatic actuation are presented in Sec. IV. Conclusions are presented in Sec. V.

II. CLASSICAL THEORY OF THERMOELASTIC DAMPING

The classical theory of thermoelastic damping has been used extensively to predict the quality factor due to ther-

 ©2006 The American Physical Society

moelastic damping, Q_{TED}, of MEMS beams and is found to give good agreement with experimental results for simple-harmonic oscillations in the flexural mode.[9,10] When a beam is flexed, one side of the beam is in tension and the other side is in compression. The side in compression gets slightly warmer and the side in tension gets slightly cooler due to the coupled nature of the thermal and mechanical domains.[16] A temperature gradient is formed across the beam giving rise to heat flow (for nonzero thermal conductivity) and this heat flow is an irrecoverable energy loss that limits the quality factor of the beam.[1]

A. Zener's theory

Zener's theory is valid for thin rectangular beams undergoing simple-harmonic vibrations in the flexural mode. According to this theory, the quality factor Q_{TED} due to thermoelastic damping is given by[1,2]

$$Q_{TED}^{-1} = \frac{E\alpha^2 T_0}{\rho C_p}\frac{\omega\tau_z}{1+(\omega\tau_z)^2} = \Delta_E \frac{\omega\tau_z}{1+(\omega\tau_z)^2}, \quad \Delta_E = \frac{E\alpha^2 T_0}{\rho C_p}, \tag{1}$$

where ρ is the density, E is the Young's modulus, α is the coefficient of thermal expansion, and C_p is the specific heat under constant pressure of the beam material. T_0 is the ambient temperature (the beam is unstrained and unstressed at this temperature) and ω is the angular frequency of excitation. τ_z is the relaxation time (the time necessary for a temperature gradient to relax) of the first mode of vibration of the beam and is given by

$$\tau_z = \frac{b^2}{\pi^2 \kappa} \tag{2}$$

where κ is the thermal diffusivity of the beam material and b is the beam thickness. When the angular frequency of excitation ω is such that $\omega\tau_z=1$, the energy loss [measured by Q_{TED}^{-1} in Eq. (1)] is maximum as the beam flexes and allows just enough time for the temperature gradient to relax before the beam changes direction (the time period of oscillation matches the relaxation time). This peak value of energy dissipation measured by Q_{TED}^{-1} in Eq. (1) is termed the "Debye peak."[3] When the angular frequency ω is much larger than the effective relaxation rate of the solid τ_z^{-1}, the system has no time to relax (the beam flexes back and forth faster than the heat can flow) and very little energy is dissipated. This is called the adiabatic regime. On the other hand when the angular frequency ω is much smaller than τ_z^{-1}, no temperature gradient is formed because the temperature gradient is proportional to the strain rate, which is low due to the low angular frequency, and very little energy is dissipated. This frequency range is called the isothermal regime. Zener's theory works quite well for simple beams but is not suitable for microstructures with complex geometries. Besides, it is also based on the assumption that the motion of the microstructure is simple harmonic.

B. Lifshitz and Roukes's theory

The Zener theory was improved in Ref. 3 by using the beam theory.[17] The equation of motion for a beam under thermoelastic damping is given by[3]

$$\rho A \frac{\partial^2 U}{\partial t^2} + \frac{\partial^2}{\partial x^2}\left(EI\frac{\partial^2 U}{\partial x^2} + E\alpha I_T\right) = 0 \tag{3}$$

where ρ is the density of the beam, A and I are the cross-sectional area and the mechanical contribution to the moment of inertia of the beam, respectively, and U is the displacement of the beam in the y direction. The x axis is defined along the length of the beam and the y and z axes are along the thickness and the width direction of the beam, respectively. The term I_T is the thermal contribution to the beam's moment of inertia (measure of the thermal stress in the beam) and is given by

$$I_T = \int_A y\theta\, dy\, dz \tag{4}$$

where $\theta=T-T_0$ is the change in the temperature from the ambient temperature T_0. The linearized heat equation (assuming $\theta \ll T_0$) along the y direction (temperature gradients along the other directions are assumed to be negligible) is given by[3]

$$\frac{\partial\theta}{\partial t} = \kappa\frac{\partial^2\theta}{\partial y^2} + y\frac{\Delta_E}{\alpha}\frac{\partial}{\partial t}\left(\frac{\partial^2 U}{\partial x^2}\right). \tag{5}$$

The coupled thermoelastic equations (3)–(5) are solved assuming simple-harmonic vibrations in Ref. 3 by setting

$$U(x,t) = U_1(x)e^{i\omega t}, \quad \theta(x,y,t) = \theta_1(x,y)e^{i\omega t}. \tag{6}$$

The temperature profile along the beam's cross section is calculated by using the heat equation (5) and the computed temperature is substituted into the equation of motion (3) to obtain a frequency-dependent elastic modulus E_ω (see Ref. 3 for details),

$$E_\omega = E\{1 + \Delta_E[1 + f(\omega)]\} \tag{7}$$

where

$$f(\omega) = \frac{24}{b^3\zeta^3}\left[\frac{b\zeta}{2} - \tan\left(\frac{b\zeta}{2}\right)\right], \quad \zeta = i\sqrt{i\frac{\omega}{\kappa}}. \tag{8}$$

The real part and the imaginary part of the frequency-dependent elastic modulus E_ω were used in Ref. 3 to compute the quality factor due to thermoelastic damping Q_{TED} as

$$Q_{TED}^{-1} = \Delta_E\left(\frac{6}{\xi^2} - \frac{6}{\xi^3}\frac{\sinh\xi + \sin\xi}{\cosh\xi + \cos\xi}\right) \tag{9}$$

where

$$\xi = b\sqrt{\frac{\omega}{2\kappa}}. \tag{10}$$

In deriving the expression for the quality factor Q_{TED}^{-1} in the Zener theory [Eq. (1)] the temperature profile in the beam was expressed in terms of the transverse thermal eigenmodes (see Refs. 1 and 2 for details). On the other hand, in the

Lifshitz and Roukes theory [Eq. (9)] the temperature profile in the beam was computed explicitly (without expanding it in terms of the thermal eigenmodes). As a result, the Lifshitz and Roukes theory is found to be more accurate than the Zener theory for predicting the quality factor due to thermoelastic damping in rectangular beams undergoing simple-harmonic vibrations in the flexural mode.[3]

III. THERMOELASTIC DAMPING IN ELECTROSTATIC MEMS

The electrostatic force is generated by applying a potential difference (combination of a dc and an ac voltage) between the microstructure and the ground plane in the MEMS device. The nonlinear nature of the electrostatic force can give rise to complex nonlinear oscillations in the MEMS device,[14,18,19] which can significantly alter the nature of thermoelastic damping from that predicted by the classical theory (both the Zener and the Lifshitz and Roukes theories) of TED. The overall quality factor Q of a MEMS device is given by

$$Q^{-1} = Q_{TED}^{-1} + Q_{fluid}^{-1} + Q_{other}^{-1} \tag{11}$$

where Q_{TED}, Q_{fluid}, and Q_{other} are the quality factors due to thermoelastic damping, fluid damping, and other sources of damping (for example, anchor damping), respectively. For MEMS beam resonators, typically Q_{fluid}^{-1} is the most dominant term in Eq. (11) under normal atmospheric conditions and determines the overall quality factor Q. At low atmospheric pressures, the value of Q_{fluid}^{-1} becomes negligible and Q_{TED}^{-1} (typically present at all pressures) becomes dominant and hence limits the overall quality factor Q of the system.[8] The effect of the electrostatic actuation force on the quality factor due to thermoelastic damping Q_{TED} is studied in this paper by using two approaches: (i) an improved form of the classical theory (the Zener and Lifshitz and Roukes theories of TED) and (ii) a coupled physical level simulation.

A. Modified theory

The theory of thermoelastic damping presented in Sec. II is modified to predict the value of Q_{TED} in electrostatic MEMS under complex nonlinear oscillations. Under electrostatic actuation, in the presence of fluid and thermoelastic damping, the equation of motion for a MEMS beam is given by

$$\rho A \frac{\partial^2 U}{\partial t^2} + c\frac{\partial U}{\partial t} + \frac{\partial^2}{\partial x^2}\left(EI\frac{\partial^2 U}{\partial x^2} + E\alpha I_T\right) = F_e = \frac{\epsilon w V^2}{2(g-U)^2} \tag{12}$$

where c is the fluid damping coefficient, ϵ is the dielectric constant of the surrounding medium, V is the applied voltage, g is the gap in the undeformed state between the beam and the ground electrode, F_e is the electrostatic force per unit length, and w is the width of the beam. A voltage of the form $V=V_{dc}+V_{ac}e^{i\omega t}$ is considered, where the real and the imaginary parts of $e^{i\omega t}$ correspond to a cosinusoidal and sinusoidal ac excitation, respectively. In the modified theory, we first solve the coupled thermoelastic equations [Eqs. (12) and (5)] by assuming

$$U(x,t) = \sum_{N=0}^{N_T} U_N(x)e^{iN\omega t}, \quad \theta(x,y,t) = \sum_{N=0}^{N_T} \theta_N(x,y)e^{iN\omega t}, \tag{13}$$

where N_T is the number of harmonics considered. Substituting Equation (13) into Equation (5) and equating the coefficients of $e^{iN\omega t}$ for $N=0, 1, 2, \ldots, N_T$ to zero gives

$$\theta_N(x,y) = \frac{\Delta_E}{\alpha}\frac{\partial^2 U_N(x)}{\partial x^2}\left(y - \frac{\sin(y\zeta_N)}{\zeta_N\cos(b\zeta_N/2)}\right) \quad \text{for } N>0; \quad \theta_0(x,y)=0; \tag{14}$$

where ζ_N is given by

$$\zeta_N = i\sqrt{\frac{iN\omega}{\kappa}}. \tag{15}$$

The thermal contribution to the beam's moment of inertia I_T can be computed from Eqs. (14), (15), and (4), [noting $\theta_0(x,y)=0$] as

$$\begin{aligned} I_T &= \int_A y\theta\, dy\, dz \\ &= \sum_{N=1}^{N_T}\int_A y\theta_N(x,y)e^{iN\omega t} dy\, dz \\ &= \sum_{N=1}^{N_T}\frac{\Delta_E I}{\alpha}[1+f(N\omega)]\frac{\partial^2 U_N(x)}{\partial x^2}e^{iN\omega t}, \end{aligned} \tag{16}$$

where $I=wb^3/12$ is the mechanical moment of inertia of the beam (of width w and thickness b) and $f(N\omega)$ is given by

$$f(N\omega) = \frac{24}{b^3\zeta_N^3}\left[\frac{b\zeta_N}{2} - \tan\left(\frac{b\zeta_N}{2}\right)\right]. \tag{17}$$

Substituting the expression for the displacement $U(x,t)$ from Eq. (13) and the expression for I_T [Eq. (16)] into Eq. (12) gives

$$\begin{aligned} &-\rho A\omega^2\sum_{N=0}^{N_T}N^2U_N(x)e^{iN\omega t} + ic\omega\sum_{N=0}^{N_T}NU_N(x)e^{iN\omega t} \\ &+ EI\sum_{N=0}^{N_T}\frac{\partial^4U_N(x)}{\partial x^4}e^{iN\omega t} + EI\Delta_E\sum_{N=1}^{N_T}[1 \\ &+ f(N\omega)]\frac{\partial^4 U_N(x)}{\partial x^4}e^{iN\omega t} = \frac{\epsilon w(V_{dc}+V_{ac}e^{i\omega t})^2}{2\left(g-\sum_{N=0}^{N_T}U_N(x)e^{iN\omega t}\right)^2}. \end{aligned} \tag{18}$$

From Eqs. (12) and (18) the bending moment[17] of the MEMS beam, M, is given by

$$M = EI\frac{\partial^2 U}{\partial x^2} + E\alpha I_T = EI\sum_{N=0}^{N_T}\frac{\partial^2 U_N(x)}{\partial x^2}e^{iN\omega t} + EI\Delta_E\sum_{N=1}^{N_T}[1+f(N\omega)]\frac{\partial^2 U_N(x)}{\partial x^2}e^{iN\omega t} = M^M + M^T \quad (19)$$

where M^M and M^T are the mechanical and the thermal contributions to the bending moment, respectively. The third and fourth terms on the left-hand side of Eq. (18) correspond to $\partial^2 M^M/\partial x^2$ and $\partial^2 M^T/\partial x^2$, respectively. The stress σ in the MEMS beam is given by[17]

$$\sigma = \frac{My}{I} = \frac{M^M y}{I} + \frac{M^T y}{I} = \sigma^M + \sigma^T \quad (20)$$

where σ^M and σ^T are the mechanical and the thermal stresses, respectively, with σ^T significantly smaller than σ^M (see Ref. 1). The strain ε in the MEMS beam is given by[17]

$$\varepsilon = y\frac{\partial^2 U}{\partial x^2} = \frac{\sigma^M}{E}. \quad (21)$$

Using the expressions for the stress and strain in the MEMS beam, the elastic potential energy stored in the system, E_{pot}, is given by[20]

$$E_{pot} = \int_V dV\int_0^{\varepsilon}\sigma\, d\varepsilon \approx \int_V dV\int_0^{\varepsilon}\sigma^M d\varepsilon, \quad (22)$$

as σ^T is negligibly small compared to σ^M and V is the volume of beam. The energy dissipated by thermoelastic damping per period of the vibration, ΔE_{TED}, is given by[2,20]

$$\Delta E_{TED} = \int_V dV \oint \sigma^T d\varepsilon \quad (23)$$

where $\oint$ signifies integration over a complete time period of vibration. The quality factor due to thermoelastic damping, Q_{TED}, of the MEMS beam can then be computed as[2]

$$Q_{TED}^{-1} = \frac{1}{2\pi}\frac{\Delta E_{TED}}{(E_{pot})_{max}} \quad (24)$$

where $(E_{pot})_{max}$ is the maximum elastic potential energy stored in the MEMS beam during one complete time period of vibration. Expressing $U_N(x)$ as[21]

$$U_N(x) = \beta_N\phi(x), \quad \text{i.e.,}\ U(x,t) = \phi(x)\sum_{N=0}^{N_T}\beta_N e^{iN\omega t}, \quad (25)$$

where $\phi(x)$ is the most dominant mode of vibration of the beam at the given frequency of excitation and β_N denotes the vibration amplitude, a closed-form expression for the quality factor Q_{TED} for the MEMS beam can be obtained as (see the Appendix for details)

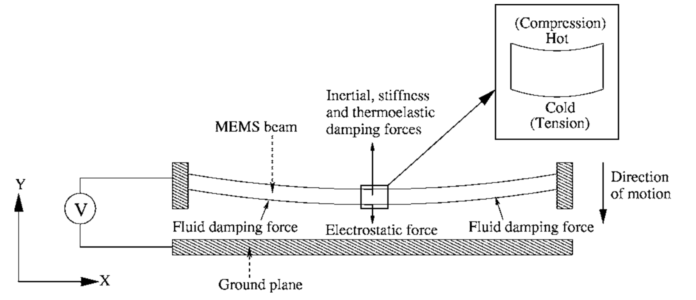

FIG. 1. Illustration of thermal-electrical-fluidic-mechanical coupling in an electrostatic MEMS through an example—a fixed-fixed MEMS beam over a ground plane: the deformed structure with the various forces acting on it when it is moving downward.

$$Q_{TED}^{-1} = \left[\sum_{N=1}^{N_T}\Delta_E\left(\frac{6}{\xi_N^2} - \frac{6}{\xi_N^3}\frac{\sinh\xi_N + \sin\xi_N}{\cosh\xi_N + \cos\xi_N}\right)N\bar{\beta}_N^2\right](\bar{\beta}_{max}^2)^{-1} \quad (26)$$

where $\bar{\beta}_N$ is the magnitude of β_N (β_N can be complex), $\bar{\beta}_{max}$ is the maximum value of the expression $\Sigma_{N=0}^{N_T}\beta_N e^{iN\omega t}$ evaluated over a time period $2\pi/\omega$, and

$$\xi_N = b\sqrt{\frac{N\omega}{2\kappa}}. \quad (27)$$

When only one harmonic ($N_T=1$) is considered in Eq. (26), i.e., for simple-harmonic motions of the beam, $\bar{\beta}_{max}=\bar{\beta}_1$, and the expression for Q_{TED} given by the modified theory [Eq. (26)] reduces to the expression for Q_{TED} given by the Lifshitz and Roukes theory [Eq. (9)].

B. Physical level analysis

A physical level simulation tool is developed in this paper for the dynamic analysis of electrostatic MEMS in the presence of fluid and thermoelastic damping. The coupling between the electrical, fluidic, and mechanical domains in electrostatic MEMS, in the absence of thermoelastic damping, is described in detail in Refs. 15, 18, and 22. In the case of thermoelastic damping, an additional damping force is present because of the temperature gradient in the microstructure due to its deformation (see Fig. 1).

Figure 1 shows a typical MEM device—a deformable fixed-fixed MEMS beam over a fixed ground plane. A potential difference V is applied between the two conductors. The applied voltage gives rise to an electrostatic force which deforms the beam. When the beam deforms, the charge redistributes on the surface of the conductors, and, consequently, the resultant electrostatic force and the deformation of the beam also change. The surrounding fluid displaced by the motion of the beam exerts a fluid damping force on the beam. The deformation of the beam also causes stress inhomogeneities within the beam which gives rise to temperature fluctuations (the side in compression gets warmer and the side in tension gets cooler) and hence a thermoelastic damping force. A self-consistent final state is reached for a given time step where the sum of all the forces (the inertial force,

the mechanical stiffness force, the fluid and thermoelastic damping forces, and the electrostatic force) is zero. The process is repeated for each time step.

A two-dimensional (2D) large-deformation thermoelastic analysis is performed for computing the mechanical deformation and the temperature profile in the microstructure on which the external electrostatic and fluidic forces act. The transient governing equations for the mechanical deformation using a Lagrangian description are given by[23,24]

$$\rho\ddot{\mathbf{u}} = \nabla \cdot (\mathbf{FS}) \quad \text{in } \Omega, \tag{28}$$

$$\mathbf{u} = \mathbf{G} \quad \text{on } \Gamma_g, \tag{29}$$

$$\mathbf{P} \cdot \mathbf{N} = \mathbf{H} \quad \text{on } \Gamma_h, \tag{30}$$

$$\mathbf{u}|_{t=0} = \mathbf{G}_0 \quad \text{in } \Omega, \tag{31}$$

$$\dot{\mathbf{u}}|_{t=0} = \mathbf{V}_0 \quad \text{in } \Omega, \tag{32}$$

where Ω is the mechanical domain, Γ_g is the portion of the boundary on which Dirichlet boundary conditions (e.g., displacement) are specified, and Γ_h is the portion of the boundary on which Neumann boundary conditions (electrostatic and fluidic pressures) are specified. ρ is the material density in the undeformed (initial) configuration, and $\mathbf{u}$, $\dot{\mathbf{u}}$, and $\ddot{\mathbf{u}}$ are the displacement, velocity, and acceleration vectors, respectively. $\mathbf{F}=\mathbf{I}+\nabla\mathbf{u}$ is the deformation gradient, and $\mathbf{S}$ is the second Piola-Kirchhoff stress given by[24]

$$\mathbf{S} = \mathbf{CE} - \frac{E\alpha}{1-\nu}\theta\mathbf{I} = \mathbf{S}^M + \mathbf{S}^T \tag{33}$$

where $\mathbf{S}^M$ and $\mathbf{S}^T$ are the mechanical and thermal components of $\mathbf{S}$, $\mathbf{C}$ is the material tensor, $\mathbf{E}=(\mathbf{F}^T\mathbf{F}-\mathbf{I})/2$ is the Green-Lagrangian strain, and ν is the Poisson ratio ($\mathbf{I}$ is the identity matrix). $\theta=T-T_0$ is the change in the temperature from the ambient temperature T_0. Equations (29) and (30) are the displacement and the surface traction boundary conditions, respectively. $\mathbf{G}$ is the prescribed displacement, and $\mathbf{N}$ is the unit outward normal vector in the initial configuration. $\mathbf{H}$ is the surface traction vector given by

$$\mathbf{H} = (P_e - P_f)J\mathbf{F}^{-T}\mathbf{N} \tag{34}$$

where P_e and P_f are the surface electrostatic and fluidic pressures, respectively, and J is the determinant of $\mathbf{F}$. $\mathbf{P}=\mathbf{FS}$ is the first Piola-Kirchhoff stress tensor. Equations (31) and (32) are the initial conditions for displacement and velocity, respectively. $\mathbf{G}_0$ and $\mathbf{V}_0$ are the initial displacement and velocity, respectively. The temperature profile T in the microstructure is obtained by solving a Lagrangian form of the heat equation,[24,25]

$$\nabla \cdot \mathbf{h} = \frac{E\alpha}{1-\nu}T\dot{e} + \rho C_p\dot{T} \quad \text{in } \Omega \tag{35}$$

where ρ is the material density in the undeformed (initial) configuration, $\mathbf{h}=J\mathbf{F}^{-1}\mathbf{q}$ is the referential heat flux vector,[25] and $\mathbf{q}$ is the heat flux in the deformed configuration, which can be computed as $\mathbf{q}=k\mathbf{F}^{-T}\nabla T$, where k is the thermal conductivity of the material. e is the sum of the diagonal components of $\mathbf{E}$ and the overdots in Eq. (35) indicate the derivatives with respect to time. A Newmark scheme with an implicit trapezoidal rule (see, for example, Ref. 26 for details) is used to solve the dynamical system posed in Eqs. (28)–(35). Numerical discretization is done by using the finite-cloud method (FCM) (see Refs. 27 and 28 for details on the FCM).

The 2D governing equation for the electrostatic analysis can be written in a boundary integral form in the Lagrangian frame (see Ref. 29 for details):

$$\phi(p(P)) = \int_{d\Omega} \frac{1}{\epsilon} G(p(P), q(Q))\sigma(q(Q))\mathbf{J}(Q)d\Gamma_Q + C, \tag{36}$$

$$\int_{d\Omega} \sigma(q(Q))\mathbf{J}(Q)d\Gamma_Q = C_T, \tag{37}$$

$$\mathbf{J}(Q) = [\mathbf{T}(Q) \cdot \mathbf{C}(Q)\mathbf{T}(Q)]^{1/2}, \tag{38}$$

where ϵ is the dielectric constant of the medium, ϕ is the electrostatic potential, and σ is the electrostatic surface charge density. P and Q are the source and field points in the initial configuration corresponding to the source and field points p and q in the deformed configuration, and G is the Green's function. In two dimensions, $G(p(P),q(Q))=-\ln|p(P)-q(Q)|/2\pi$, where $|p(P)-q(Q)|$ is the distance between the source point $p(P)$ and the field point $q(Q)$. C_T is the total charge of the system and C is an unknown variable which can be used to compute the potential at infinity. $\mathbf{T}(Q)$ is the tangential unit vector at field point Q and $\mathbf{C}(Q)$ is the Green deformation tensor. Equations (36)–(38) are solved using the boundary-cloud method (BCM) (see Refs. 30 and 31 for details on the BCM) to obtain the distribution of surface charge density σ on the conductors. The electrostatic pressure normal to the surface of the conductors is given by

$$P_e = \frac{\sigma^2}{2\epsilon}. \tag{39}$$

Reynold's squeeze film equation (RSFE) is used to compute the fluid or air damping pressure acting on the MEM structure. The RSFE is applicable for structures where a small gap between two plates opens and closes with respect to time,[32] like, for example, the MEMS fixed-fixed beam resonator over a ground plane shown in Fig. 1. A Lagrangian form of the isothermal Reynold squeeze film equation for compressible slip flow is given by[18,33]

$$\mathbf{F}^{-T}\nabla \cdot [(1+6K)h^3P_f\mathbf{F}^{-T}\nabla P_f] = 12\eta\frac{\partial(P_fh)}{\partial t}, \tag{40}$$

where h is the gap between the movable structure (for example the fixed-fixed beam in Fig. 1) and the ground plane of the MEM device (the same as the fluid film thickness), P_f is the fluid pressure under the structure, and η is the viscosity of the surrounding fluid. $K=\lambda/h$ is the Knudsen number, where λ is the mean free path of the surrounding fluid. Numerical discretization of the RSFE is done by using the

finite-cloud method and time integration is done using a Crank-Nicholson scheme (see Ref. 18 for more details on the solution of the RSFE for electrostatic MEMS). A self-consistent solution of the coupled electrostatic, fluidic, and thermoelastic analysis at each time step is obtained using a Newton method.

The quality factor Q_{TED} in the physical level analysis is also computed using Eq. (24). The potential energy stored in the system is the elastic potential energy and in this case is given by[26]

$$E_{pot} = w\int_A \left(\sum_{i,j=1}^{2} \frac{1}{2} s_{ij}^M e_{ij}\right) dA \tag{41}$$

where s_{ij}^M are the components of $\mathbf{S}^M$. The relatively insignificant thermal stress $\mathbf{S}^T$ compared to the mechanical stress $\mathbf{S}^M$ is neglected in the computation of the potential energy. e_{ij} are the components of $\mathbf{E}$, w is the width of the microstructure, and A is the area of the microstructure (the 2D domain where the mechanical analysis is done). The energy dissipated by thermoelastic damping ΔE_{TED} is given by[20]

$$\Delta E_{TED} = w\int_A \oint \left(\sum_{i,j=1}^{2} s_{ij}^T de_{ij}\right) dA \tag{42}$$

where $\oint$ signifies integration over a complete time period of vibration and s_{ij}^T are the components of the thermal stress $\mathbf{S}^T$. Equations (24), (41), and (42) are used to compute the quality factor due to thermoelastic damping in the MEMS devices in Sec. IV.

IV. RESULTS

Two different sources of nonlinearity in the electrostatic force per unit length, F_e, can be identified from the beam equation for electrostatic MEMS [Eq. (12)] and they are (i) $F_e \propto V^2$ and (ii) $F_e \propto 1/(g-U)^2$. These nonlinearities in F_e can give rise to complex nonlinear vibrations in the MEMS beam (discussed later and also presented in Refs. 14, 18, and 19). The effect of these nonlinear vibrations on Q_{TED} is studied in this section using the modified theory and the physical level analysis, for MEMS fixed-fixed beams of different geometries. The results obtained from the classical theory of thermoelastic damping are also discussed.

A. Model validation

The physical level simulation tool is used to simulate a set of MEMS cantilever beams[9] to determine the thermoelastic damping ratio $\delta = 1/(2Q_{TED})$ at the resonant frequency for $T_0 = 300$ K. The dimensions of the five different cantilever beams (corresponding to the five experimental data points in Fig. 2) and their relaxation times (τ_z) computed using Eq. (2) are shown in Table I.

The beams are made of silicon and have the following materials properties:[9] $\alpha = 2.6\times10^{-6}$ K^{-1}, $E = 170$ GPa, $\nu = 0.3$, $\rho = 2330$ kg m^{-3}, $C_p = 712$ J kg^{-1} K^{-1}, $k = \kappa\rho C_p = 148$ W m^{-1} K^{-1}, where k is the thermal conductivity.

The resonators (cantilever beams) were placed in a vacuum chamber which eliminates gas damping and a very small excitation force was applied to prevent any nonlinear oscillations in the system.[9] The damping ratio is independent of the excitation force for very small magnitudes of the excitation force in the linear regime. Figure 2 shows the variation in the damping ratio of the resonators with the resonant frequency f. Comparisons between the experimentally measured data, the numerical simulations, and the modified theory are shown in Fig. 2. The resonant frequency of each beam (f) is normalized with respect to the characteristic damping frequency $f_d = 1/(2\pi\tau_z)$ of the beam. A dc bias of 0.1 V along with an ac bias of 0.01 V is used in the simulations and the modified theory to generate an electrostatic actuation force in the linear regime.

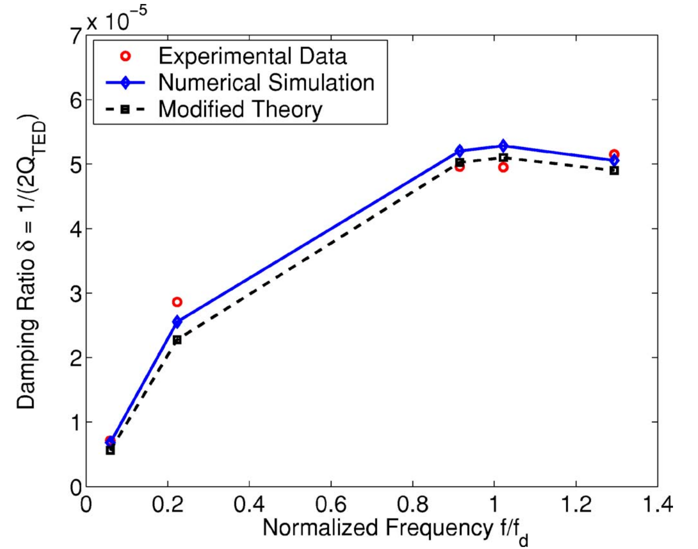

FIG. 2. (Color online) Comparisons between the measured and the computed (numerical simulations and modified theory) damping ratio δ for five cantilever beams (Ref. 9) in vacuum. $f_d = 1/(2\pi\tau_z)$ is the characteristic damping frequency.

Figure 3 shows the comparison between the measured and computed (both the numerical simulations and the modified theory) quality factor Q_{TED} for a set of silicon fixed-fixed[13] beams in vacuum at $T_0 = 300$ K. The length of the fixed-fixed beam was changed to obtain different resonant frequencies and the thickness was kept constant at 5 μm. The five experimental data points in Fig. 3 were obtained from 5-μm-thick fixed-fixed beams of lengths 700 μm (at its first and third resonant frequencies, 80.3 and 490 kHz, respectively), 500 μm (at its third resonant frequency 720 kHz), and 200 μm (at its first and third resonant frequencies, 911

TABLE I. Cantilever beam dimensions (from Ref. 9).

Beam No.	Length (μm)	Thickness (μm)	Width (μm)	τ_z (μs)
Beam 1	395	10	54	0.1136
Beam 2	192	10	54	0.1136
Beam 3	183	15	27	0.255
Beam 4	204	17.5	27	0.3478
Beam 5	190	17.5	54	0.3478

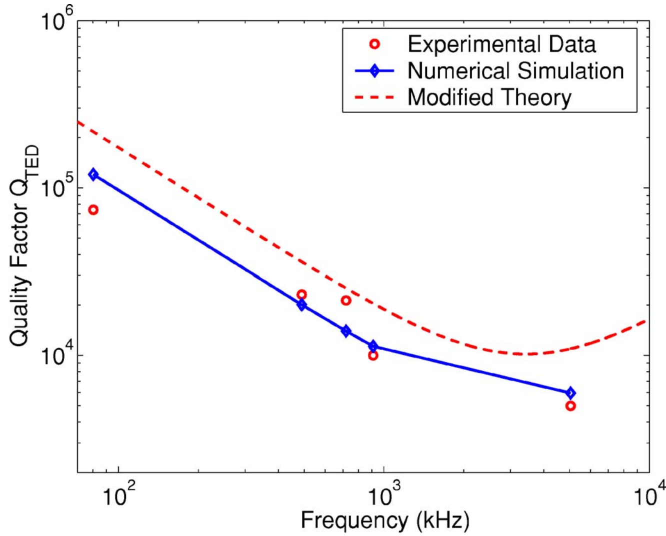

FIG. 3. (Color online) Comparisons between the measured and the computed (numerical simulations and modified theory) quality factor Q_{TED} for a set of silicon fixed-fixed beams (Ref. 13) in vacuum.

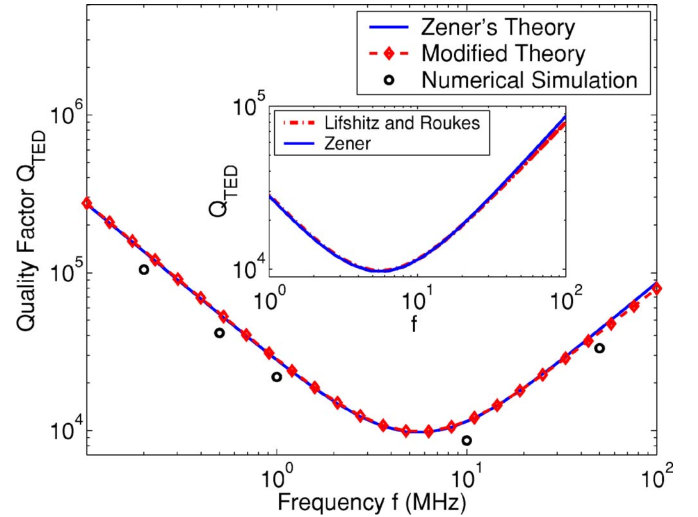

FIG. 4. (Color online) Variation of Q_{TED} with the excitation frequency f for the MEMS fixed-fixed beam A (resonant frequency is f_0=1.08 MHz) under dc operations ($r \to 0$) obtained from the different theories and numerical simulation. Characteristic damping frequency is f_d=5.6 MHz, where Q_{TED} is minimum.

and 5.05 MHz, respectively). The beams have the following material properties:[13] $\alpha=2.6\times10^{-6}$ K^{-1}, $E=130$ GPa, $\nu=0.28$, $\rho=2330$ kg m^{-3}, $C_p=712$ J kg^{-1} K^{-1}, $k=\kappa\rho C_p=148$ W m^{-1} K^{-1}. A dc bias of 0.1 V along with an ac bias of 0.01 V is used in the numerical simulations and the modified theory to generate an electrostatic actuation force in the linear regime. The numerically simulated values of Q_{TED} and those obtained from the modified theory are close to the experimental data for both the cantilever beams and the fixed-fixed beams as shown in Figs. 2 and 3.

B. Effect of the $F_e \propto V^2$ nonlinearity

When the applied voltage V is small (compared to the pull-in voltage of the MEMS beam), the displacement $U \ll g$ and the nonlinearity due to $F_e \propto 1/(g-U)^2$ is negligible [see Eq. (12)]. However, the nonlinearity due to $F_e \propto V^2$ can still be present at such small voltages and give rise to different values of Q_{TED} than that predicted by the classical theory of thermoelastic damping.[1,3] Considering an applied voltage of the form $V=V_{dc}+V_{ac}\sin(\omega t)$, where V_{dc} is the applied dc bias and $V_{ac}\sin(\omega t)$ is the sinusoidal ac voltage, the electrostatic force per unit length F_e will have both the first and the second harmonics of the exciting angular frequency ω due to the V^2 nature, i.e.,

$$F_e \approx \frac{\epsilon w}{2g^2}\left(V_{dc}^2 + \frac{V_{ac}^2}{2} + 2V_{dc}V_{ac}\sin(\omega t) - \frac{V_{ac}^2}{2}\cos(2\omega t)\right). \tag{43}$$

Defining $r=V_{ac}/(V_{dc}+V_{ac})$, $r=1$ (when $V_{dc}=0$) implies ac operation (when the second harmonic of the exciting angular frequency ω is dominant) and $r \to 0$ (when $V_{ac} \ll V_{dc}$) implies dc operation (when the first harmonic is dominant). For intermediate values of r between 0 and 1 (mixed-mode operation) both the first and the second harmonic components of the applied voltage are dominant. The effect of the different modes of operation (ac, dc, and mixed mode) on thermoelastic damping in MEMS is studied for a fixed-fixed MEMS beam (denoted as beam A) at T_0=300 K. The fixed-fixed MEMS beam (beam A) considered is made from silicon and has dimensions $200\times5\times10$ μm^3 (length$\times$thickness$\times$width), placed 1 μm over a ground plane. The material properties used are the same as those used for the cantilever beams in Sec. IV A and the beam's resonant frequency is f_0=1.08 MHz. The relaxation time of the beam is $\tau_z=0.0284$ μs [computed using Eq. (2)] giving a characteristic damping frequency $f_d=1/(2\pi\tau_z)$ (the frequency where TED is maximum, i.e., Q_{TED} is minimum) of 5.6 MHz. The beam is simulated in air at 1 atm ($\eta=1.82\times10^{-5}$ kg/ms and the mean free path $\lambda=0.064$ μm). Figure 4 shows the variation in Q_{TED} with the excitation frequency $f=\omega/(2\pi)$ for the fixed-fixed beam A, under dc operations (V_{dc}=1 V and V_{ac}=0.0001 V, $r \to 0$) obtained using the Zener theory, the modified theory, and the numerical simulations.

The fluid damping coefficient (needed in the modified theory) $c=0.0205$ N s/m^2 is obtained from the linearized Reynold squeeze film theory[34] for beam A. The value of Q_{TED} obtained from the Zener theory, the modified theory, and the numerical simulation are very close as shown in Fig. 4 (the numerical simulation results are typically more accurate due to its 2D analysis as compared to the theories, which are based on 1D analysis of the system[13]). Under dc operations at small voltages where the nonlinearity due to $F_e \propto 1/(g-U)^2$ is negligible, the motion of the beam is simple harmonic at the excitation frequency f. In this case, the Zener theory and the Lifshitz and Roukes theory (compared with the Zener theory in the inset of Fig. 4) match the modified theory and are very close to the numerical simulations. The pull-in voltage of the fixed-fixed beam is found to be 120 V, thereby indicating that the applied voltages are very small. The inset of Fig. 4 shows some minor variations be-

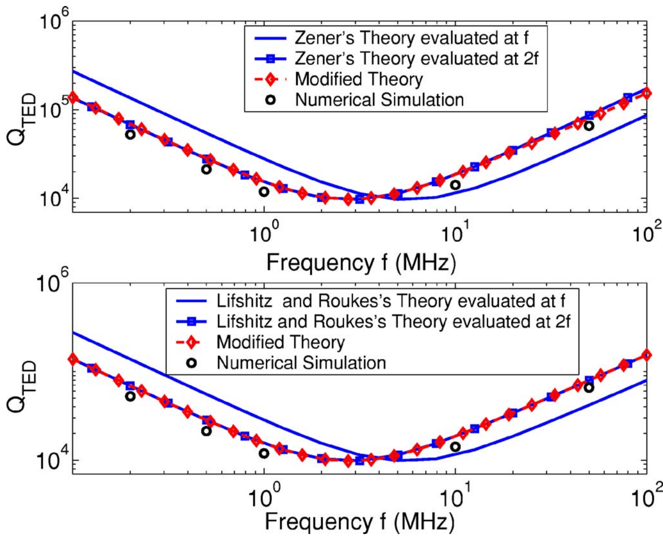

FIG. 5. (Color online) Variation of Q_{TED} with the excitation frequency f for the MEMS fixed-fixed beam A under ac operations (r=1) obtained from the different theories and numerical simulation. Characteristic damping frequency is f_d=2.8 MHz, where Q_{TED} is minimum.

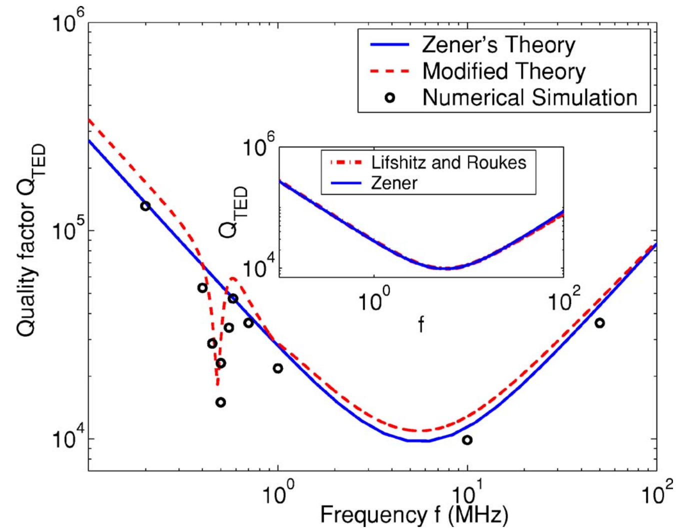

FIG. 6. (Color online) Variation in Q_{TED} with the excitation frequency f for the MEMS fixed-fixed beam A (resonant frequency is f_0=1.08 MHz) under mixed-mode operation at r=0.5 (V_{dc}=0.5 V, V_{ac}=0.5 V), obtained from the different theories and numerical simulation.

tween the Zener theory and the Lifshitz and Roukes theory at higher frequencies which is consistent with the observations made in Ref. 3. Note that the modified theory is identical to the Lifshitz and Roukes theory when only one harmonic (N_T=1) is considered in Eq. (26), i.e., for simple-harmonic motions of the beam.

For ac operations (V_{dc}=0 V and V_{ac}=1 V, r=1), the value of Q_{TED} obtained from the Zener and the Lifshitz and Roukes theories evaluated at $\omega=2\pi f$ does not match the predictions of the modified theory or the numerical simulations as shown in Fig. 5. However, the classical theories evaluated at $2\omega=2\pi(2f)$ agree well with the modified theory (and the results are close to those of the numerical simulations) as the oscillations are still simple harmonic but at twice the excitation frequency due to the V^2 nature of F_e under ac operations from Eq. (43). In this case, the characteristic damping frequency is found to be half of that in the dc operation, i.e., f_d=2.8 MHz as shown in Fig. 5. While minor variations can be observed between the Zener model evaluated at $2\omega=2\pi(2f)$ and the modified theory at higher frequencies in Fig. 5, the value of Q_{TED} given by Lifshitz and Roukes theory evaluated at $2\omega=2\pi(2f)$ is found to be exactly the same as the modified theory at all the frequencies. For mixed-mode operations (intermediate values of r between 0 and 1), the electrostatic force per unit length F_e contains both the first and the second harmonic components of the exciting frequency [see Eq. (43)]. As a result, the oscillations also have both these two frequency components in them, giving rise to nonsimple harmonic oscillations. The value of the quality factor due to thermoelastic damping, Q_{TED}, for such cases cannot be predicted correctly by the classical theories as shown in Fig. 6.

Figure 6 shows the variation in Q_{TED} with the excitation frequency f for a mixed-mode operation at V_{dc}=0.5 V and V_{ac}=0.5 V, r=0.5 in the fixed-fixed beam A. While the modified theory and the numerical simulations indicate the formation of a spike in the downward direction in Q_{TED} around $f_0/2$ (f_0=1.08 MHz is the resonant frequency of the beam), no such predictions are made by the Zener or the Lifshitz and Roukes theory. The formation of the spike in Q_{TED} around $f_0/2$ can be explained from the variation in the magnitudes of β_1 and β_2 [Eq. (25)] with the excitation frequency f for the fixed-fixed beam at V_{dc}=0.5 V and V_{ac}=0.5 V (r=0.5). While the magnitude of the first harmonic β_1 peaks at the resonant frequency of the system as expected, the second harmonic β_2 becomes dominant (larger than β_1) at $f_0/2$ as shown in Fig. 7. Since the quality factor Q_{TED} depends on the relative strengths of the different harmonics present [see Eq. (26)], maximum deviation between the classical theories (based on the first harmonic) and the modified theory and numerical simulations is observed at $f_0/2$ where the second harmonic is most dominant.

Similar observations were also made for another MEMS fixed-fixed beam (beam B) of different geometry. The fixed-fixed beam B is made from silicon (same material properties as beam A) and has dimensions $80\times2\times10\ \mu\text{m}^3$ (length $\times$thickness$\times$width), placed 0.5 μm over a ground plane and is simulated under similar ambient conditions as beam A.

The relaxation time is τ_z=0.0045 μs and the characteristic damping frequency is 35 MHz. The pull-in voltage of beam B is found to be 69 V dc and the resonant frequency is f_0=2.72 MHz. The fluid damping coefficient for the beam B is c=0.062 N s/m^2 (used in the modified theory). Figure 8 shows the variation in Q_{TED} with the excitation frequency f for the fixed-fixed beam B under ac operations (r=1) obtained from the different theories and numerical simulation. Figure 9 shows the variation in Q_{TED} with the excitation frequency f under mixed-mode operation at r=0.5 (V_{dc}=0.5 V, V_{ac}=0.5 V), obtained from the different theories and numerical simulation. Zener's theory shows similar devia-

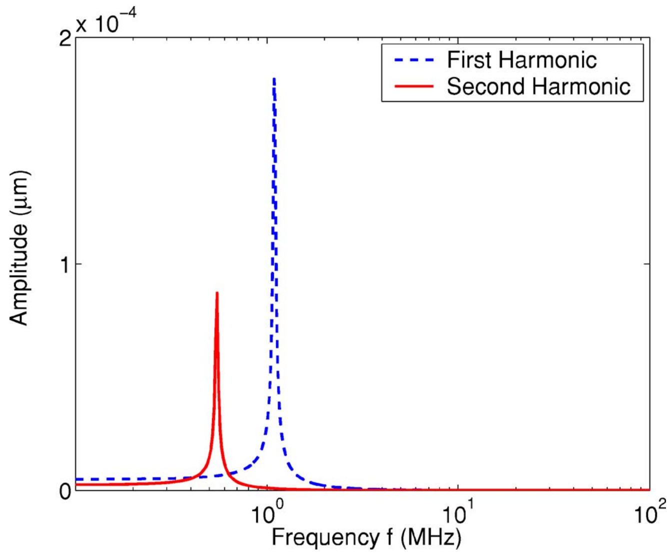

FIG. 7. (Color online) Amplitude variation of the first and the second harmonics, β_1 and β_2, respectively, with the excitation frequency f for the MEMS fixed-fixed beam A at $r=0.5$ ($V_{dc}=0.5$ V, $V_{ac}=0.5$ V).

tions from the modified theory and the numerical simulations for beam B as observed in beam A. The results from the Lifshitz and Roukes theory are very similar to those of the Zener theory and are not shown here.

C. Effect of the $F_e \propto 1/(g-U)^2$ nonlinearity

When the applied voltages are large, the displacement U is comparable with the gap g and the nonlinearity due to $F_e \propto 1/(g-U)^2$ in Eq. (12) becomes important.[14] The effect of the $F_e \propto 1/(g-U)^2$ nonlinearity on the quality factor due to thermoelastic damping, Q_{TED}, is studied in this section for the two fixed-fixed beams presented in Sec. IV B, namely, beams A and B. Figure 10 shows the variation in Q_{TED} with the normalized frequency f/f_0 for the fixed-fixed beam A at 100 V dc (close to the pull-in voltage) and 5 V ac. The resonant frequency of the beam A at 100 V dc is $f_0=893$ kHz. The quality factor Q_{TED} (computed by the modified theory and also by the numerical simulations) has several spikes in its variation with respect to the normalized frequency f/f_0 as shown in Fig. 10. The spikes occur at the superharmonics of the resonant frequency f_0, i.e., at $f=f_0/N$ for $N=1,2,3,\ldots,$ and are not predicted by the Zener or the Lifshitz and Roukes theory (not shown here as it gives very similar results as the Zener theory).

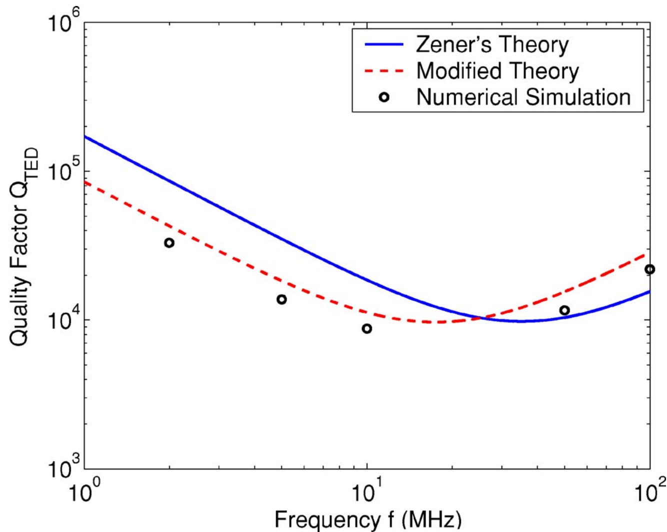

FIG. 8. (Color online) Variation in Q_{TED} with the excitation frequency f for the MEMS fixed-fixed beam B (resonant frequency is $f_0=2.72$ MHz) under ac operations ($r=1$) obtained from the different theories and numerical simulation. The characteristic damping frequency is 17.6 MHz (half of that in the dc operation).

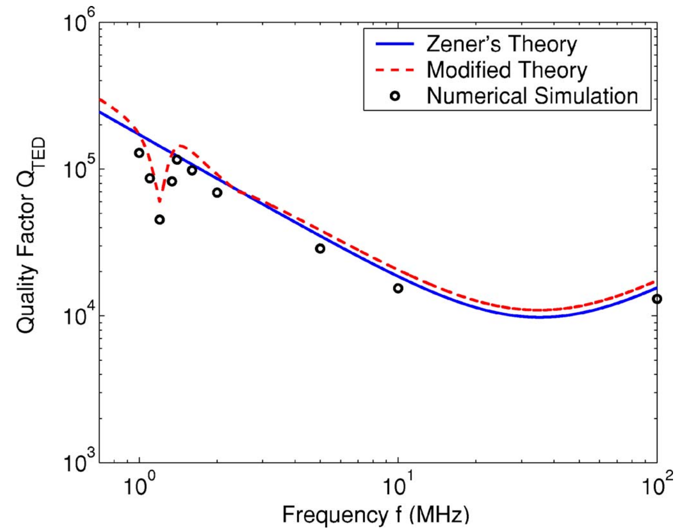

FIG. 9. (Color online) Variation in Q_{TED} with the excitation frequency f for the MEMS fixed-fixed beam B under mixed-mode operation at $r=0.5$ ($V_{dc}=0.5$ V, $V_{ac}=0.5$ V), obtained from the different theories and numerical simulation.

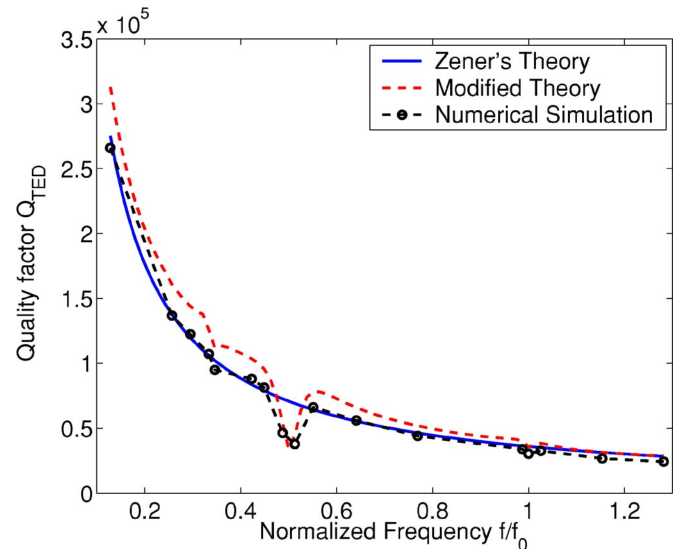

FIG. 10. (Color online) Variation in Q_{TED} with the normalized frequency f/f_0 for the fixed-fixed beam A at 100 V dc (close to the pull-in voltage) and 5 V ac. The resonant frequency at 100 V dc is $f_0=893$ kHz.

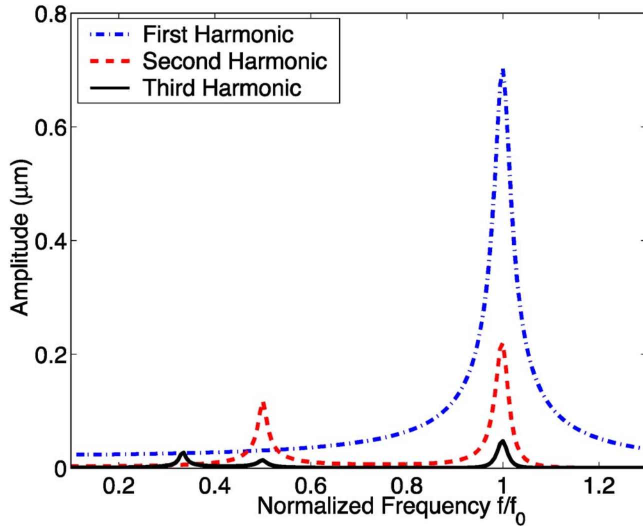

FIG. 11. (Color online) Amplitude variation of the first three harmonics, β_1, β_2, and β_3, with the normalized frequency f/f_0 for the fixed-fixed beam A at 100 V dc (close to the pull-in voltage) and 5 V ac.

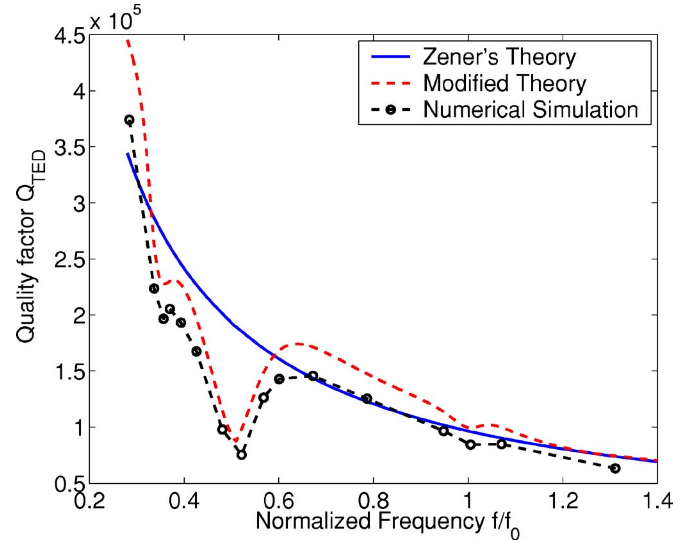

FIG. 12. (Color online) Variation in Q_{TED} with the normalized frequency f/f_0 for the fixed-fixed beam B at 60 V dc (close to the pull-in voltage) and 5 V ac. The resonant frequency at 60 V dc is f_0=1.785 MHz.

The formation of the spikes in Fig. 10 can be explained by the presence of higher-order harmonics in the oscillations introduced by the $F_e \propto 1/(g-U)^2$ nonlinearity at higher voltages (close to pull in). Harmonic balance analysis of the beam equation [Eq. (12)] shows the presence of several higher-order harmonics in the oscillations of beam A at 100 V dc and 5 V ac as shown in Fig. 11. The magnitude of the Mth harmonic β_M [Eq. (25)] is found to peak or spike at the first M superharmonic frequencies of f_0, i.e., at $f=f_0/N$ for $N=1,2,3,\ldots,M$. This in turn affects the quality factor Q_{TED} at a given frequency as shown in Fig. 10 as the quality factor Q_{TED} at a given frequency depends on the relative strengths of the different harmonics β_N present [from Eq. (26)].

The formation of spikes in the thermoelastic quality factor Q_{TED} versus normalized excitation frequency f/f_0 plot at larger voltages is also observed in beam B. Figure 12 shows the variation in Q_{TED} with the normalized frequency f/f_0 for the fixed-fixed beam B at 60 V dc (close to the pull-in voltage of 69 V dc) and 5 V ac. The resonant frequency of the beam B at 60 V dc is f_0=1.785 MHz. Figure 13 shows the presence of several higher-order harmonics in the oscillations of the MEMS beam B at 60 V dc and 5 V ac resulting in formation of the spikes in Q_{TED}.

The strength of the harmonics β_N decreases very rapidly with increasing N (see Ref. 18) and the quality factor Q_{TED} computed using the modified theory is found to converge by considering a finite number of harmonics. For example, the number of harmonics used in the modified theory for both beams A and B in this paper is N_T=10. Figures 10 and 12 show that the quality factor of the MEMS beams is affected by the application of higher dc voltages not only at the superharmonic frequencies but also at their resonant frequencies, i.e., at f/f_0=1, which is the most commonly used excitation frequency for microstructures.

V. CONCLUSIONS

The nonlinear nature of the electrostatic actuation force is found to change the nature of thermoelastic damping in electrostatic MEMS significantly from that predicted by the classical theory of thermoelastic damping developed by Zener and later improved by Lifshitz and Roukes. The nonlinearity due to the V^2 nature of the electrostatic force is found to affect the thermoelastic quality factor Q_{TED} even at small voltages (far from pull in). At larger voltages (closer to pull in), the nonlinearity due to the $1/(g-U)^2$ nature of the electrostatic force is found to affect Q_{TED}. A modified theory is proposed for predicting thermoelastic damping in MEMS under arbitrary electrostatic actuation. The modified theory

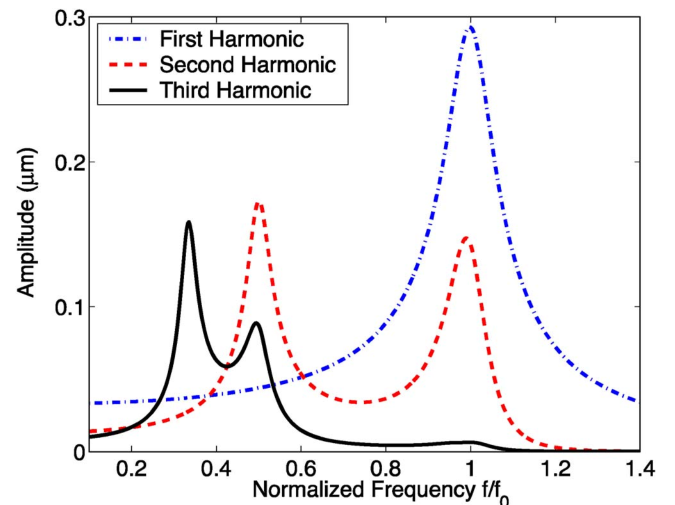

FIG. 13. (Color online) Amplitude variations of the first three harmonics, β_1, β_2, and β_3, with the normalized frequency f/f_0 for the fixed-fixed beam B at 60 V dc (close to the pull-in voltage) and 5 V ac.

takes into account the higher-order harmonics present in the oscillations, which arise due to nonlinear electrostatic forces, to compute the overall thermoelastic damping coefficient and the quality factor. Although the quality factor Q_{TED} predicted by the modified theory is close to the numerical simulation predictions, typically the physical level or numerical simulations based on the coupled 2D nonlinear electrical-thermal-mechanical-fluidic analysis are more accurate as they involve fewer assumptions compared to the modified theory.

ACKNOWLEDGMENTS

This work is supported by the National Science Foundation under Grants No. 0121616, No. 0217986, No. 0228390, and No. 0601479.

APPENDIX: DERIVATION OF Q_{TED}

After substituting Eq. (25) into Eq. (18), a harmonic balance analysis[21] is performed to compute β_N for $N=0,1,2,\ldots,N_T$. The thermal contribution to the bending moment M^T is negligible compared to the mechanical contribution to the bending moment M^M.[1] As a result, the vibration amplitudes β_N of the different harmonics can be computed by neglecting the term $\partial^2 M^T/\partial x^2$ in Eq. (18) and by replacing $U_N(x)$ by $\beta_N\phi(x)$ to obtain

$$\left(-\rho A\omega^2\sum_{N=0}^{N_T}N^2\beta_N e^{iN\omega t}+ic\omega\sum_{N=0}^{N_T}N\beta_N e^{iN\omega t}\right)\phi(x)+EI\frac{\partial^4\phi(x)}{\partial x^4}\sum_{N=0}^{N_T}\beta_N e^{iN\omega t}=\frac{\epsilon w(V_{dc}+V_{ac}e^{i\omega t})^2}{2\left(g-\phi(x)\sum_{N=0}^{N_T}\beta_N e^{iN\omega t}\right)^2}. \tag{A1}$$

The mode shape of vibration $\phi(x)$ for a beam is given by[26]

$$\phi(x)=\cosh(qx)-\cos(qx)+p[\sinh(qx)-\sin(qx)] \tag{A2}$$

where p and q depend on the beam type (cantilever or fixed-fixed) and on the order of the mode and resonant frequency. From Eq. (A2)

$$\frac{\partial^4\phi(x)}{\partial x^4}=q^4\phi(x). \tag{A3}$$

Using Eq. (A3), rearranging the terms, and integrating Eq. (A1) along the length of the beam gives

$$\left(\sum_{N=0}^{N_T}R_N\beta_N e^{iN\omega t}\right)\left[\bar{A}g^2+\bar{B}\left(\sum_{N=0}^{N_T}\beta_N e^{iN\omega t}\right)^2-2\bar{C}g\sum_{N=0}^{N_T}\beta_N e^{iN\omega t}\right]=\frac{\epsilon wL(V_{dc}+V_{ac}e^{i\omega t})^2}{2} \tag{A4}$$

where L is the length of the beam,

$$R_N=-\rho A\omega^2N^2+ic\omega N+EIq^4, \tag{A5}$$

and

$$\bar{A}=\int_0^L\phi(x)dx,\quad \bar{B}=\int_0^L\phi^3(x)dx,\quad \bar{C}=\int_0^L\phi^2(x)dx. \tag{A6}$$

Equating the coefficients of e^0 to zero in Eq. (A4) gives

$$\bar{B}R_0\beta_0^3-2g\bar{C}R_0\beta_0^2+\bar{A}g^2R_0\beta_0-\frac{\epsilon wLV_{dc}^2}{2}=0, \tag{A7}$$

from which a closed form expression for β_0 can be obtained. Equating the coefficients of $e^{iN\omega t}$ for $N=1,2,\ldots,N_T$ to zero in Eq. (A4) gives

$$\beta_1=\frac{\epsilon wLV_{dc}V_{ac}}{\bar{A}g^2R_1+\bar{B}R_1\beta_0^2+2\bar{B}R_0\beta_0^2-2\bar{C}gR_0\beta_0-2\bar{C}gR_1\beta_0}, \tag{A8}$$

$$\beta_2=\frac{\epsilon wLV_{ac}^2/2-\bar{B}R_0\beta_0\beta_1^2-2\bar{B}R_1\beta_0\beta_1^2+2\bar{C}gR_1\beta_1^2}{\bar{A}g^2R_2+\bar{B}R_2\beta_0^2+2\bar{B}R_0\beta_0^2-2\bar{C}gR_0\beta_0-2\bar{C}gR_2\beta_0}, \tag{A9}$$

$$\beta_Q=\left[-\bar{B}\sum_{N=0}^{Q-1}R_N\beta_N\beta_{Q/2-N/2}^2-2\bar{B}\left(R_0\beta_0\bar{\Gamma}(Q)+\sum_{N=1}^{Q-1}R_N\beta_N\Gamma(Q-N)\right)+2\bar{C}g\sum_{N=1}^{Q-1}R_N\beta_N\beta_{Q-N}\right]\times[\bar{A}g^2R_Q+\bar{B}R_Q\beta_0^2+2\bar{B}R_0\beta_0^2-2\bar{C}g(R_0\beta_0+R_Q\beta_0)]^{-1}\quad \text{for } Q=3,\ldots,N_T \tag{A10}$$

where $\Gamma(I)$ is the summation of the combination of all possible pairs $\beta_J\beta_K$ for $J+K=I$ and $J<K$ and $\bar{\Gamma}(I)$ is exactly the same as $\Gamma(I)$ but does not include the term $\beta_0\beta_I$ in the summation. $\beta_P=0$ if P is a fraction.

The maximum potential energy of the MEMS beam, $(E_{pot})_{max}$, during one time period of the vibration, can be computed using Eqs. (21) and (22) as

$$(E_{pot})_{max}=\int_V dV\int_0^{\varepsilon_{max}}\sigma^M d\varepsilon=\int_V dV\int_0^{\varepsilon_{max}}E\varepsilon\, d\varepsilon=\frac{Ew}{2}\int_{-t/2}^{t/2}\int_0^L\varepsilon_{max}^2dx\,dy \tag{A11}$$

where w and L are the beam width and length, respectively, and ε_{max} is given by

$$\varepsilon_{max}=y\left|\frac{\partial^2U(x,t)}{\partial x^2}\right|_{max}=y\frac{\partial^2\phi(x)}{\partial x^2}\left|\sum_{N=0}^{N_T}\beta_N e^{i\omega Nt}\right|_{max}=y\frac{\partial^2\phi(x)}{\partial x^2}\bar{\beta}_{max} \tag{A12}$$

where $\bar{\beta}_{max}$ is the maximum value of the expression

$\Sigma_{N=0}^{N_T}\beta_N e^{iN\omega t}$ evaluated over a time period $2\pi/\omega$. Integrating over the volume of the MEMS beam, V, the expression for the peak potential energy becomes

$$(E_{pot})_{max} = \frac{EI\bar{\beta}_{max}^2}{2}\left[\int_0^L \left(\frac{\partial^2\phi(x)}{\partial x^2}\right)^2 dx\right]. \quad \text{(A13)}$$

The energy dissipated per period by thermoelastic damping can be computed using Eq. (23):

$$\Delta E_{TED} = \int_V dV \oint \sigma^T d\varepsilon = w\int_{-t/2}^{t/2}\int_0^L \oint \sigma^T d\varepsilon\, dx\, dy \quad \text{(A14)}$$

where σ^T is given by Eq. (20) as

$$\sigma^T = \frac{M^T y}{I} = yE\Delta_E \sum_{N=1}^{N_T}[1+f(N\omega)]\frac{\partial^2 U_N(x)}{\partial x^2}e^{i\omega Nt} = yE\Delta_E \frac{\partial^2\phi(x)}{\partial x^2}\sum_{N=1}^{N_T}\beta_N[1+f(N\omega)]e^{i\omega Nt}. \quad \text{(A15)}$$

In Eq. (A14), $d\varepsilon$ can be written as

$$d\varepsilon = d\left(y\frac{\partial^2 U(x,t)}{\partial x^2}\right) = i\omega y\sum_{N=0}^{N_T}\frac{\partial^2 U_N(x)}{\partial x^2}Ne^{i\omega Nt}dt = i\omega y\frac{\partial^2\phi(x)}{\partial x^2}\sum_{N=0}^{N_T}\beta_N N e^{i\omega Nt}dt. \quad \text{(A16)}$$

From Eqs. (A14)–(A16), the energy dissipated per cycle by thermoelastic damping, ΔE_{TED}, can be obtained as

$$\Delta E_{TED} = EI\Delta_E\pi\left[\int_0^L\left(\frac{\partial^2\phi(x)}{\partial x^2}\right)^2 dx\right]\sum_{N=1}^{N_T} \times\left(\frac{6}{\xi_N^2} - \frac{6}{\xi_N^3}\frac{\sinh\xi_N + \sin\xi_N}{\cosh\xi_N + \cos\xi_N}\right)N\bar{\beta}_N^2 \quad \text{(A17)}$$

where $\bar{\beta}_N$ is the magnitude of β_N and

$$\xi_N = b\sqrt{\frac{N\omega}{2\kappa}}, \quad \text{(A18)}$$

which gives the expression for the quality factor Q_{TED} for the MEMS beam as

$$Q_{TED}^{-1} = \left[\sum_{N=1}^{N_T}\Delta_E\left(\frac{6}{\xi_N^2} - \frac{6}{\xi_N^3}\frac{\sinh\xi_N + \sin\xi_N}{\cosh\xi_N + \cos\xi_N}\right)N\bar{\beta}_N^2\right][\bar{\beta}_{max}^2]^{-1}. \quad \text{(A19)}$$

[1] C. Zener, Phys. Rev. **52**, 230 (1937).
[2] C. Zener, Phys. Rev. **53**, 90 (1938).
[3] R. Lifshitz and M. L. Roukes, Phys. Rev. B **61**, 5600 (2000).
[4] H. Luo, G. Zhang, L. R. Carley, and G. K. Fedder, J. Microelectromech. Syst. **11**, 188 (2002).
[5] N. Yazdi, F. Ayazi, and K. Najafi, Proc. IEEE **86**, 1640 (1998).
[6] M. S. Weinberg, B. T. Cunningham, and C. W. Clapp, J. Microelectromech. Syst. **9**, 370 (2000).
[7] C. T.-Nguyen, in *Proceedings of the Ultrasonics Symposium, Seattle, WA, 1995* (IEEE, New York, 1995), p. 489.
[8] A. Duwel, J. Gorman, M. Weinstein, J. Borenstein, and P. Ward, Sens. Actuators, A **103**, 70 (2003).
[9] T. V. Roszhart, in *Proceedings of the Solid-State Sensor and Actuator Workshop, Hilton Head Island, SC, 1990* (IEEE, New York, 1990), p. 13.
[10] K. Y. Yasumura, T. D. Stowe, E. M. Chow, T. Pfafman, T. W. Kenny, B. C. Stipe, and D. Rugar, J. Microelectromech. Syst. **9**, 117 (2000).
[11] V. T. Srikar and S. D. Senturia, J. Microelectromech. Syst. **11**, 499 (2002).
[12] R. Abdolvand, H. Johari, G. K. Ho, A. Erbil, and F. Ayazi, J. Microelectromech. Syst. **15**, 471 (2006).
[13] S. Pourkamali, A. Hashimura, R. Abdolvand, G. K. Ho, A. Erbil, and F. Ayazi, J. Microelectromech. Syst. **12**, 487 (2003).
[14] S. K. De and N. R. Aluru, Phys. Rev. Lett. **94**, 204101 (2005).
[15] S. K. De and N. R. Aluru, J. Microelectromech. Syst. **13**, 737 (2004).
[16] W. Nowacki, *Thermoelasticity* (Pergamon Press, Oxford, 1986).
[17] E. G. Popov, *Engineering Mechanics of Solids* (Prentice-Hall, Englewood Cliffs, NJ, 1997).
[18] S. K. De and N. R. Aluru, J. Microelectromech. Syst. **15**, 355 (2006).
[19] S. K. De and N. R. Aluru, Proc. R. Soc. London, Ser. A **462**, 3435 (2006).
[20] A. S. Nowick and B. S. Berry, *Anelastic Relaxation in Crystalline Materials* (Academic Press, New York, 1972).
[21] A. T. Nayfeh and D. T. Mook, *Nonlinear Oscillations* (John-Wiley and Sons, New York, 1979).
[22] S. K. De and N. R. Aluru, J. Micromech. Microeng. **16**, 1705 (2006).
[23] D. S. Chandrasekharaiah and L. Debnath, *Continuum Mechanics* (Academic Press, New York, 1994).
[24] H. Parkus, *Thermoelasticity* (Blaisdell Publishing Company, New York, 1968).
[25] P. Yarrington and D. E. Carlson, Int. J. Eng. Sci. **14**, 113 (1976).
[26] K. J. Bathe, *Finite Element Procedures* (Prentice-Hall, Englewood Cliffs, NJ, 1995).
[27] N. R. Aluru and G. Li, Int. J. Numer. Methods Eng. **50**, 2373 (2001).
[28] X. Jin, G. Li, and N. R. Aluru, Comput. Struct. **83**, 1366 (2005).
[29] G. Li and N. R. Aluru, J. Microelectromech. Syst. **11**, 245 (2002).
[30] G. Li and N. R. Aluru, Comput. Methods Appl. Mech. Eng. **191**,

2337 (2002).
[31] G. Li and N. R. Aluru, Eng. Anal. Boundary Elem. **27**, 57 (2003).
[32] J. B. Starr, in *Proceedings of the Solid-State Sensor and Actuator Workshop, Hilton Head Island, SC, 1990* (IEEE, New York, 1990), p. 44.
[33] A. Burgdorfer, J. Basic Eng. **81**, 94 (1959).
[34] J. M. Huang, K. M. Liew, C. H. Wong, S. Rajendran, M. J. Tan, and A. Liu, Sens. Actuators, A **93**, 273 (2001).